



Detection of an Unstable Intermediate in Br^- Electro-oxidation to Br_3^- on a Platinum Electrode in Nitrobenzene by Scanning Electrochemical Microscopy



Jinho Chang¹, Brent Bennett*, Allen J. Bard

Department of Chemistry and Biochemistry, Center for Electrochemistry, The University of Texas at Austin, Austin, TX 78712, United States

ARTICLE INFO

Article history:

Received 11 January 2017

Received in revised form 7 March 2017

Accepted 1 April 2017

Available online 3 April 2017

Keywords:

scanning electrochemical microscopy

electrochemistry

bromine

nitrobenzene

reaction mechanism

intermediate detection

cyclic voltammetry

digital simulation

ABSTRACT

We report the detection of an unstable intermediate generated during Br^- oxidation to Br_3^- in nitrobenzene by scanning electrochemical microscopy (SECM), and we attempt to simulate the collection of the intermediate using a proposed mechanism of Br^- oxidation to Br_3^- . At a distance of $\sim 3.5 \mu\text{m}$ between the tip and the substrate electrode in the SECM experiment, we observed two waves as we measured the collection efficiency, N_{ss} , while holding the tip at an anodic potential and scanning the substrate toward cathodic potentials. The second wave obtained at more negative substrate potentials was associated with the collection of Br_3^- , and the first wave was associated with the collection of an intermediate generated in Br^- oxidation to Br_3^- . The N_{ss} as a function of d , estimated at the constant substrate potential of 0.27 V vs. $\text{TMPD}/\text{TMPD}^{\cdot+}$, abruptly increased as d was brought below $2.5 \mu\text{m}$. We simulated this approach curve by using the following mechanism of Br^- oxidation to Br_3^- : (1) $\text{Br}^- + e \rightleftharpoons \text{Br}\cdot$, (2) $2\text{Br}\cdot \rightleftharpoons \text{Br}_2$, (3) $\text{Br}\cdot + \text{Br}^- \rightleftharpoons \text{Br}_2^{\cdot-}$, (4) $\text{Br}_2^{\cdot-} + e \rightleftharpoons \text{Br}_2$, and (5) $\text{Br}_2 + \text{Br}^- \rightleftharpoons \text{Br}_3^-$.

© 2017 Elsevier Ltd. All rights reserved.

1. Introduction

In this paper, we report evidence of an unstable intermediate generated from Br^- oxidation to Br_3^- in nitrobenzene (NB) through scanning electrochemical microscopy (SECM). Several research groups have studied Br^- electro-oxidation to Br_2 via a highly stable Br_3^- in nonaqueous solvents for decades Kolthoff and Coetzee [1] and Popov and Geske [2] reported $\text{Br}^-/\text{Br}_3^-/\text{Br}_2$ oxidation in acetonitrile (MeCN) on a Pt rotating disk electrode (RDE). Iwasita and Giordano [3] did similar work in acetonitrile and nitromethane [4], and Vojinovic et al. [5] studied bromide oxidation and bromine reduction in propylene carbonate. Bontempelli's group [6] studied the reaction on a Pt sphere microelectrode, and Behl [7] reported bromide oxidation in tetrahydrofuran (THF) on both Pt and GC rotating ring-disk electrodes. Mastragostino et al. [8] proposed a mechanism for bromide and chloride oxidation in anhydrous acetic acid. Boon et al. performed a study of bromide oxidation in

low-temperature bromoaluminate molten salts [9]. More recently, studies of Br^- oxidation have been done in room temperature ionic liquids on Pt electrodes. Allen et al. studied the oxidation of bromide in acetonitrile and in 1-butyl-3-methylimidazolium bis(trifluoromethylsulfonyl)imide [10,11], and Yu et al. [12] compared bromide and chloride oxidation in 1-butyl-3-methylimidazolium hexafluorophosphate.

In those reports, the authors proposed the reaction pathway of Br^- oxidation to Br_3^- via either $\text{Br}\cdot$ dimerization [6,10,13] to Br_2 (Tafel mechanism) or through the addition of a Br^- ion to Br followed by the addition of an electron to form Br_2 (Heyrovsky mechanism) [5,6,10,11,13]. The latter reaction may occur simultaneously or in a two step-process through the intermediate, $\text{Br}_2^{\cdot-}$. In either case, the Br_2 picks up Br^- to form stable Br_3^- . In all of these reports, the high stability of Br_3^- was given as the reason why Br^- oxidation to Br_2 occurs in two successive waves, instead of the single wave seen in aqueous systems. Although these pathways have been widely proposed, direct experimental evidence to confirm any of the proposed mechanisms, such as detection of the diffusive unstable intermediates, $\text{Br}\cdot$, Br_2 or $\text{Br}_2^{\cdot-}$, has not been reported.

Since Bard et al. [14] invented SECM, it has been used as a powerful tool to detect unstable intermediates generated from electrochemical reactions because of its high collection efficiency

* Correspondence to: Materials Science and Engineering Program, The University of Texas at Austin, Austin, Texas 78712, United States. Tel.: +14325280899; fax: 512.471.0088.

E-mail address: brent.bennett@utexas.edu (B. Bennett).

¹ Current Address: Department of Chemistry, Sungshin W. University, 55 Dobong-ro, 76ga-gil, Gangbuk-gu, Seoul 01133, Republic of Korea.

and low detection limit. Among many successful examples of this application, Mirkin et al. [15] observed the intermediate BH_3 in borohydride oxidation, Zhou et al. [16] detected the acrylonitrile radical as an intermediate in its reduction, and Bi et al. [17] reported the guanosine radical in its oxidation. Recently, Cao et al. [18] reported the detection of *N,N*-dimethylaniline (DMA) cation radical during the electro-oxidation of DMA in acetonitrile. The primary advantages of SECM over fast scan cyclic voltammetry are [18,19]: (1) electrochemical measurements are performed in the absence of capacitance, and thus, a lower detection limit is obtained; (2) collected current on the substrate is only from diffusive species generated at the tip, and any surface induced reactions (adsorption/desorption) cannot perturb the analysis of diffusion controlled reactions. Therefore, more clear evidence of the diffusive intermediate can be obtained.

Another motivation for this study is to explore the possibility of using the Br^-/Br_2 redox couple in non-aqueous redox flow batteries. The redox flow battery (RFB) has emerged as a promising solution to the need for large-scale energy storage that can enable the electrical grid to respond to increasing electricity consumption and renewable energy generation [20–22]. Among the many candidates for redox couples in aqueous RFBs, the Br^-/Br_2 redox couple has been widely used because of its large positive redox potential (+1.08 V vs. NHE in aqueous solution) and its two electron transfer behavior. The high energy density of the Br^-/Br_2 redox couple is a major advantage of aqueous RFB systems such as zinc/bromine and bromine/polysulfide [21]. For these same reasons, this redox couple would appear to be a promising candidate for the positive electrode reaction in a variety of non-aqueous RFBs. After all, recent interest in non-aqueous electrolytes for RFBs has been primarily motivated by the pursuit of wider voltage windows and higher energy densities than what is possible in aqueous systems [23–26]. However, as stated above, the Br^-/Br_2 reaction is a two-step irreversible process in most non-aqueous solvents. Therefore, we hope that this mechanistic study of the Br^-/Br_2 redox couple will uncover ways to catalyze the reaction and make it more reversible.

In this study, we chose nitrobenzene (NB) as our solvent, instead of more common solvents such as MeCN, for several reasons. First, we are currently studying the possibility of creating a high energy density RFB using NB and Br_2 . It has been reported that NB undergoes a reversible one-electron transfer with $E_{1/2} = -1.05$ V vs. SCE and $E_{1/2} \sim -1$ V vs. a Ag quasi-reference electrode, with some variation in the potential depending on the primary solvent being used [27–30]. We believe that NB could be used as a negative redox couple and as a solvent in an RFB system. Second, NB has low volatility relative to many other solvents and has a relatively high dielectric constant ($\epsilon = 34.8$). Also, water and oxygen have low solubility in NB and are easier to remove from it than other solvents such as acetonitrile. Finally, bromine and many tribromide salts are highly soluble in NB and do not react with it [31].

2. Experimental details

2.1. Chemicals

For the SECM experiments, nitrobenzene (99 +%, ACS reagent), tetraethylammonium tetrafluoroborate (TEABF_4 , 99 +%), and tetraethylammonium bromide (TEABr , 99 +%) were obtained from Acros Organics (Somerville, NJ) and used without further purification. For the cyclic voltammetry (CV) and chronoamperometry experiments, which are shown in the Supporting Information, further purification was required in order to reduce the amount of water and oxygen. NB was purged for 20 min with Ar and placed in an Ar-filled glovebox with O_2 levels and H_2O

levels maintained below 5 ppm. Inside the glovebox, the NB was shaken with alumina, activated at 500 °C for 9 hours, in order to remove dissolved H_2O . TEABF_4 and TEABr were dried at 100–120 °C under vacuum for at least 4 hours. Bromine (Br_2 , 99.5 +% ACS reagent) and *N,N,N,N'*-tetramethyl-*p*-phenyldiamine (TMPD, 99%) were obtained from Sigma-Aldrich and used without further purification. All electrochemical measurements were performed in NB with 0.1 M TEABF_4 as a supporting electrolyte.

2.2. Instruments and measurements

All electrochemical measurements were performed using a CH 920C SECM station bipotentiostat and a CH 660D potentiostat (CH Instruments, Austin, TX) for SECM and CV, respectively, using a three electrode configuration: Pt disks with different radii, a (1 mm, 50, 25, and 5 μm), as working electrodes; a Pt wire as a counter electrode; and an Ag wire as a quasireference electrode (QRE). To help stabilize the reference electrode, the Ag wire was placed in a glass tube filled with 0.1 M TEABF_4 and capped with a VYCOR[®] porous glass frit. The reference potential was stable to within 10 mV over the course of one day, but it could fluctuate more dramatically over the course of weeks, especially when the solution inside the tube was changed. Therefore, all potentials were referenced against the redox potential of $\text{TMPD}/\text{TMPD}^+$, which was +0.23 V to +0.33 V vs. Ag QRE.

All CV and chronoamperometric experiments were performed either inside an MBraun Unilab 2000 Glovebox (Stratham, NH), where $T = 30 \pm 1$ °C, or outside the glovebox in a sealed tube (ambient $T = 20$ °C) in order to avoid contamination from atmospheric water and oxygen. All SECM experiments were performed inside a laboratory chemical hood ($T = 25$ °C) outside the glovebox because vibrations inside the glovebox made it difficult to approach the tip and substrate electrodes close to each other.

2.3. Pt electrodes

A 1 mm radius Pt electrode was obtained from CH Instruments and used for CV experiments at slower scan rates (≤ 1 V/s). In order to reduce the capacitance and IR distortion in CV experiments at fast scan rates (≥ 10 V/s), Pt ultramicroelectrodes (UMEs) with $a = 5$ were used. To make the UMEs, Pt (99.99%) wires from Goodfellow (Devon, PA) were sealed in borosilicate capillaries from FHC (Bowdoin, ME) with an outer diameter of 1.5 mm and an inner diameter of 0.75 mm. Pt UMEs with $a = 25$ μm were made in the same manner and used for chronoamperometry experiments. All of the Pt electrodes were polished using aqueous alumina slurries containing successively smaller particles (1 and 0.3 μm) and thoroughly rinsed to remove the alumina particles before the experiments. In chronoamperometry and CV, Pt UMEs were used without a decrease in RG (the ratio of the radii of an insulating material and a metal wire). In the SECM experiments, Pt UMEs were sharpened to make a RG of 1.1 – 2 in order to move the tip close to a substrate electrode without touching the two electrodes.

2.4. Simulation

Computational simulation for SECM was performed with COMSOL v4.2a (COMSOL Inc., Burlington, MA), and diffusion problems were solved by the finite element method [32] under a steady-state condition. The simulation space was depicted in 2D axial symmetrical mode, as described in Fig. S1, with $a_{\text{Tip}} = 5$ μm and $a_{\text{Sub}} = 50$ μm .

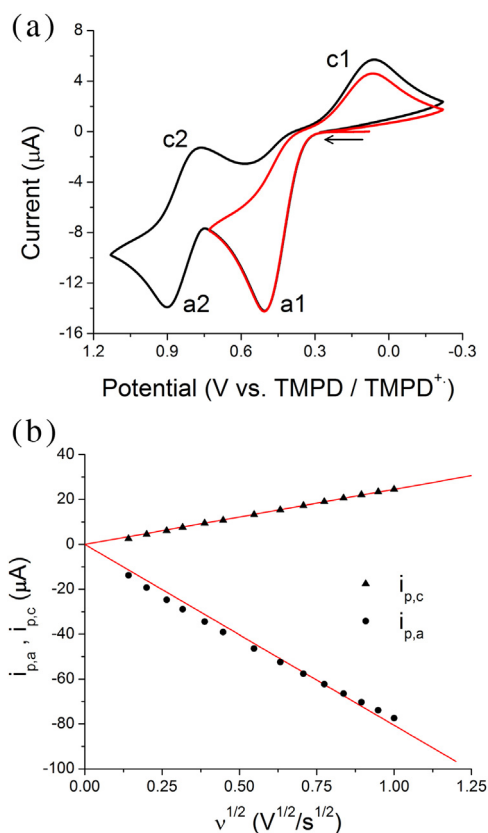


Fig. 1. (a) CVs obtained from a 10 mM TEABr in NB solution at $\nu = 0.02$ V/s on a Pt macroelectrode ($a = 1$ mm). The red line represents the CV of the $\text{Br}^-/\text{Br}_3^-$ redox reaction, and the black line is the full Br^-/Br_2 reaction. (b) A plot showing the linear relationship between the peak currents, $i_{p,a1}$ and $i_{p,c1}$, and $\nu^{1/2}$ for Br^- oxidation and Br_3^- reduction.

3. Results and discussion

3.1. Reaction overview and diffusion coefficients

Fig. 1a shows a CV obtained in NB solution with 10 mM Br^- at a scan rate of $\nu = 0.02$ V/s on a Pt macroelectrode ($a = 1$ mm). The voltammetric behavior is similar to those observed in MeCN [1,2] and THF solution [5]. The first wave (**a1/c1**) is attributed to the $\text{Br}^-/\text{Br}_3^-$ redox reaction (Reaction 1) and the second wave (**a2/c2**) to the $\text{Br}_3^-/\text{Br}_2$ reaction (Reaction 2);



In this paper, we only focus on the first redox reaction, $\text{Br}^-/\text{Br}_3^-$. Additional CV data, using both 1 mm and 5 μm radius Pt electrodes at scan rates ranging from 0.02 V/s to 500 V/s, can be found in Figs. S8–S10.

Fig. 1b shows the peak currents of the oxidation and reduction peaks, **a1** and **c1**, vs. $\nu^{1/2}$, and the corresponding peak current, $i_{p,a}$ and $i_{p,c}$, was linearly proportional to $\nu^{1/2}$, indicating the oxidation and reduction reactions are both diffusion-controlled, following the Randles-Sevcik equation [33];

$$i_{p,a} (\text{or } i_{p,c}) = (2.69 \times 10^5) n^3 A D_{\text{Br}^-}^{1/2} \left(\text{or } D_{\text{Br}_3^-}^{1/2} \right) C_{\text{Br}^-}^* \left(\text{or } C_{\text{Br}_3^-}^* \right) \nu^{1/2} \quad (3)$$

where n is the electron number, D_{Br^-} and $D_{\text{Br}_3^-}$ are the diffusion coefficients of Br^- and Br_3^- , and $C_{\text{Br}^-}^*$ and $C_{\text{Br}_3^-}^*$ are the bulk concentrations of Br^- and Br_3^- , respectively. The unresolved two electron transfer characteristics of the Br^- oxidation reaction indicates the existence of rapid chemical reactions coupled with electron transfer steps [19].

The diffusion coefficients of Br^- , Br_3^- , and Br_2 , namely D_{Br^-} , $D_{\text{Br}_3^-}$, and D_{Br_2} , were measured through chronoamperometry using a Pt UME by applying a procedure described in a previously reported paper [34]. The data is shown in Figs. S2 and S3 in the Supporting Information, and a summary of the procedure is given on page S-5 after the figures. D_{Br^-} was calculated to be $4.0 (\pm 0.2) \times 10^{-6} \text{ cm}^2/\text{s}$, and this value was used for D_{Br^-} in the simulation because it is not possible to measure the D of such a short-lived intermediate using this technique. We similarly found $D_{\text{Br}_3^-} = 5.1$

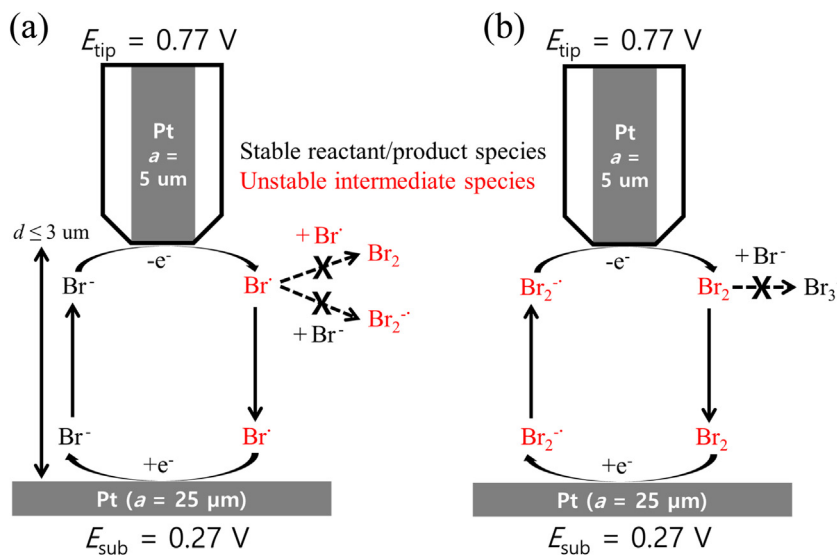


Fig. 2. Schematic descriptions of the collection of possible intermediates, (a) $\text{Br}\cdot$ and (b) $\text{Br}_2\cdot^-$, generated during Br^- oxidation in TG/SC mode of SECM. The species marked as black represents stable species and one as red represents unstable intermediates in bromide solution. The proposed mechanism of Br^- oxidation to Br_3^- is described in Scheme 1.

(± 0.2) $\times 10^{-6}$ cm²/s during Br₃⁻ reduction and $D_{\text{Br}_3^-} = 5.5 (\pm 0.1) \times 10^{-6}$ cm²/s during Br₃⁻ oxidation. We used a value of 5.5×10^{-6} cm²/s because that value fit well with the simulation and with the measured steady-state current at a 5 μm radius UME. D_{Br_2} was measured to be $1.0 (\pm 0.2) \times 10^{-6}$ cm²/s. The trend of $D_{\text{Br}_2} < D_{\text{Br}_3^-} < D_{\text{Br}_2}$ is consistent with previously reported data for the Br⁻/Br₃⁻/Br₂ system in acetonitrile [2].

3.2. Scanning electrochemical microscopy (SECM)

As mentioned above, Br⁻ electro-oxidation to Br₃⁻ involves chemical reactions coupled with electron transfer reactions, which generates unstable intermediates. Detection of these intermediates can elucidate the electro-oxidation pathway of Br⁻ to Br₃⁻. Fig. 2 shows schematic descriptions for the collection of Br⁻ (Fig. 2a) and Br₂ (Fig. 2b) intermediates, which both may be generated during Br⁻ oxidation to Br₃⁻. On a tip Pt UME ($a_{\text{tip}} = 5 \mu\text{m}$), the tip potential, E_{tip} , was scanned for Br⁻ oxidation to Br₃⁻ while different substrate potentials, E_{sub} , were held on a substrate Pt UME ($a_{\text{sub}} = 50 \mu\text{m}$) to collect the diffusive electro-active species generated on the tip. When the tip electrode is far from the substrate electrode, and the lifetime of intermediates is shorter than the time for them to diffuse on the substrate ($t_{\text{diff}} = d^2/2D$, where d is the tip-substrate distance), only the stable species, Br₃⁻ can be reduced to Br⁻ on the substrate electrode. However, when the tip electrode is close enough to make t_{diff} shorter than the lifetime of the intermediates, those intermediates can be also reduced on the substrate electrode.

Before every experiment, d was adjusted using positive feedback generated from a stable and electrochemically reversible TMPD/TMPD⁺ redox reaction in NB solution. An explanation of this method is shown in Figs. S4 and S5 and the accompanying paragraph. This distance calibration was necessary because there was always a difference between the distance that was inputted into the computer and the distance the SECM tip actually moved, resulting from a hysteresis in the stepper motor that caused the tip to recoil slightly after we stopped moving it. After adjusting $d \sim 3.5 \mu\text{m}$, the NB solution with TMPD was changed to 5 or 10 mM Br⁻ in NB solution without touching the tip and substrate electrode.

Fig. 3a shows CV_{tip} and CV_{sub} obtained by scanning E_{tip} from 0.07 to 0.77 V and constantly applying $E_{\text{sub}} = 0.37$ V. The CV_{sub} shows a constant reduction current, -1.4 nA, which was mainly associated with Br⁻ electro-oxidation on the substrate electrode. This background reduction current observed in CV_{sub} was subtracted to show the collection behavior more clearly, and the CVs_{tip} and the background-subtracted CVs_{sub} at different E_{sub} are shown in Fig. 3b. The collection current, which cannot be associated with Br₃⁻ reduction, was clearly seen in the CVs_{sub} when E_{tip} was increased from 0.47 to 0.77 V. Fig. 3c shows the collection efficiency, N_{ss} , estimated by measuring i_{T} and i_{S} from the CVs_{tip} and CVs_{sub} at different E_{sub} . The estimated N_{ss} increased from 0.14 to 0.19 as E_{sub} was decreased from 0.37 to 0.3 V, and reached a plateau until E_{sub} was 0.245 V (region I). As E_{sub} was brought more negative than 0.245 V, N_{ss} increased significantly, and approached unity (region II) as shown in the inset of Fig. 3c.

The N_{ss} polarization curve at region II was well matched with the reduction peak (c1) region observed in the CV in Fig. 1a, and thus, the N_{ss} curve shown in region II was attributed to the electro-reduction of Br₃⁻ to Br⁻. The N_{ss} curve at region I, however, cannot be entirely associated with Br₃⁻ electro-reduction because E_{sub} was too positive to reduce enough Br₃⁻ to account for that collection efficiency. Therefore, the N_{ss} observed in the region I is indicative of the collection of intermediates generated during Br⁻ oxidation. The N_{ss} for collection of intermediates could not be estimated for $E_{\text{sub}} > 0.37$ V because the anodic current associated with Br⁻ oxidation

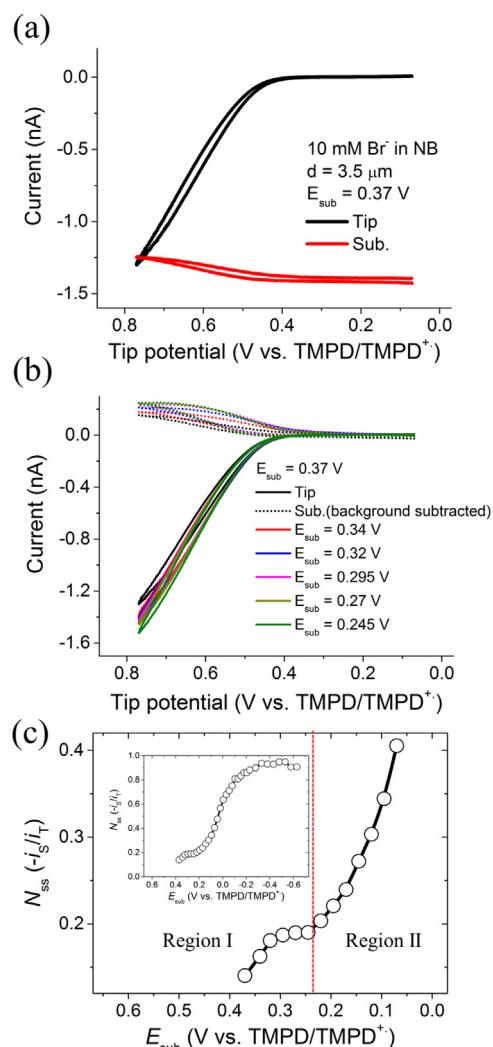


Fig. 3. (a) TG (black)/SC (red) CVs at $E_{\text{sub}} = 0.37$ V, (b) TG (solid lines)/SC (dotted lines) CVs at $0.245 \leq E_{\text{sub}} \leq 0.37$ V, (c) N_{ss} from measuring i_{T} and i_{S} at $E_{\text{tip}} = 0.77$ V and $0.245 \leq E_{\text{sub}} \leq 0.37$ V, and (inset) N_{ss} at $-0.63 \leq E_{\text{sub}} \leq 0.37$ V. All CVs were performed in 10 mM Br⁻ solution at 0.02 V/s.

was significantly higher than the current attributed to the reduction of intermediates.

In order to further confirm that the N_{ss} polarization curve in the region I was attributed to an unstable intermediate reduction, the N_{ss} at $E_{\text{sub}} = 0.27$ V was estimated as d was decreased. The N_{ss} should increase as d decreases because an intermediate can be collected more easily as explained above. Fig. 4a shows CVs_{tip} and CVs_{sub} obtained in NB solution with 10 mM Br⁻ at different d , and $E_{\text{sub}} = 0.27$ V [35]. As d decreased, i_{T} decreased significantly due to the blocking of Br⁻ diffusion from a bulk solution into the gap between the tip and substrate electrode. i_{S} also decreased as d became smaller, but i_{S} decreased less than i_{T} . Fig. 4b shows N_{ss} of intermediates estimated by measuring i_{T} and i_{S} at $E_{\text{tip}} = 0.77$ V with different d . An abrupt increase of the N_{ss} at a dimensionless tip-substrate distance $L (= d/a) \leq 0.8$ was clearly observed, indicating that more intermediates were being collected on the substrate electrode as d decreased. Even at $1 \leq L \leq 1.6$, cathodic currents were observed in the CVs_{sub}, and N_{ss} shows only a slight increase as L decreased down to 1: $N_{\text{ss}} = 0.16$ at $L = 1.6$, $N_{\text{ss}} = 0.17$ at $L = 1$. The N_{ss} shown at $1 \leq L \leq 1.6$ was mainly associated with a Br₃⁻ collection on the substrate. Since Br₃⁻ is a stable species in NB solution with Br⁻, the N_{ss} associated with Br₃⁻ collection was subtracted from the total N_{ss} as a baseline (red line in Fig. 4b). CVs_{tip} and CVs_{sub}

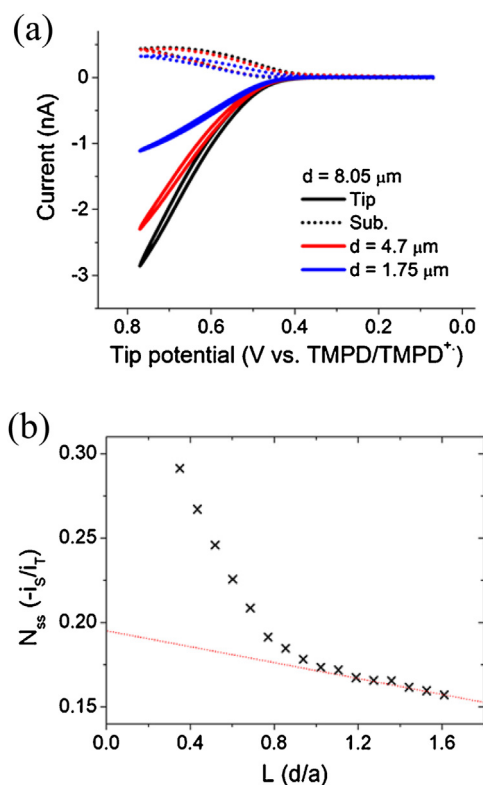
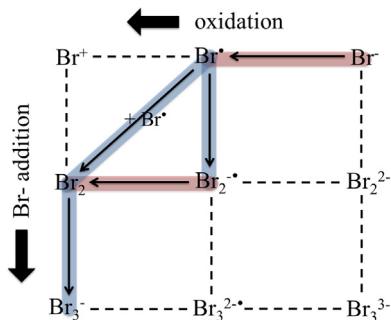


Fig. 4. (a) TG/SC CVs at different d (8.05, 4.7, and 1.75 μm), $E_{\text{sub}} = 0.27\text{ V}$, $v = 0.02\text{ V/s}$ in 10 mM Br^- solution, and (b) corresponding N_{ss} obtained from measuring i_T and i_S at $E_{\text{tip}} = 0.77\text{ V}$ in the TG/SC CVs vs. L .

obtained in NB with 5 mM Br^- at different d , $E_{\text{sub}} = 0.27\text{ V}$, and the corresponding N_{ss} as a function of d are also shown in Fig. S6.

3.3. SECM simulations and Br^- oxidation mechanism

We also chose to model the collection efficiency of the intermediate in COMSOL using the following mechanism, also shown in Scheme 1, to support our experimental findings. The reaction parameters, which are listed in Table 1 along with confidence intervals, are based on CV simulations from a previous study of this reaction [36].



Scheme 1. Description of the reaction mechanism used in the SECM simulation of Br^- oxidation. Blue shaded lines are chemical steps involving the addition of either a Br^- ion or a Br^\cdot radical to the initial species, and red shaded lines are heterogeneous electron transfer steps. The dotted lines indicate possible reactions that are not included in the simulation and are shown here simply for illustration. The reaction parameters, along with confidence intervals, are given in Table 1.

Table 1

Reaction parameters with confidence intervals for the SECM simulation in Fig. 5. The label “no limit” under the high and low columns indicates that we could not determine a point at which the value of that parameter had a visible effect on the simulation. More detailed information regarding the COMSOL simulation is given in Table S1.

Reactions and parameters for SECM simulation			
		High	Low
$\text{Br}^\cdot + e^- \rightleftharpoons \text{Br}_2^{\cdot-}$	$E^\circ = 0.63\text{ V}$ $\alpha = 0.3$ $k_s = 0.2\text{ cm s}^{-1}$	0.70 V 0.5 1.0 cm s^{-1}	0.60 V 0.1 0.05 cm s^{-1}
$\text{Br}^\cdot + \text{Br}^- \rightleftharpoons \text{Br}_2^{\cdot-}$	$k_{f,1} = 5.0 \times 10^4\text{ M}^{-1}\text{ s}^{-1}$	$1.0 \times 10^5\text{ M}^{-1}\text{ s}^{-1}$	$1.0 \times 10^4\text{ M}^{-1}\text{ s}^{-1}$
$\text{Br}^\cdot + \text{Br}^\cdot \rightleftharpoons \text{Br}_2$	$k_{f,2} = 4.0 \times 10^7\text{ M}^{-1}\text{ s}^{-1}$	$5.0 \times 10^7\text{ M}^{-1}\text{ s}^{-1}$	$3.0 \times 10^7\text{ M}^{-1}\text{ s}^{-1}$
$\text{Br}_2 + e^- \rightleftharpoons \text{Br}_2^{\cdot-}$	$E^\circ = 0.59\text{ V}$ $\alpha = 0.3$ $k_s = 0.01\text{ cm s}^{-1}$	1.0 V no limit no limit	-0.1 V no limit no limit
$\text{Br}^- + \text{Br}_2 \rightleftharpoons \text{Br}_3^-$	$k_{f,3} = 1.0 \times 10^{10}\text{ M}^{-1}\text{ s}^{-1}$	no limit	$1.0 \times 10^8\text{ M}^{-1}\text{ s}^{-1}$



Fig. 5 shows the baseline subtracted N_{ss} obtained by tip generation (TG)/substrate collection (SC) mode in SECM at different Br^- concentrations, 5 and 10 mM, as a function of d . The X marks and overlaid circles represent experimental and simulated results, respectively. At both Br^- concentrations, the N_{ss} associated with intermediate collection increased when L was less than 0.8, and reached ca. 0.12 at $L = 0.3$. There are two general discrepancies between the experimental and simulated approach curves that can be traced to probable sources of error in the experiment. First is the fact that the simulated curves are slightly steeper than the experimental curves, which may be caused in part by error in measuring the small intermediate collection current ($N_{\text{ss}} \sim 0.1$) against a larger background current ($N_{\text{ss}} \sim 0.2$). Second is error in the d measurement, which we believe causes the two approach curves for 5 mM Br^- and 10 mM Br^- to overlap more than

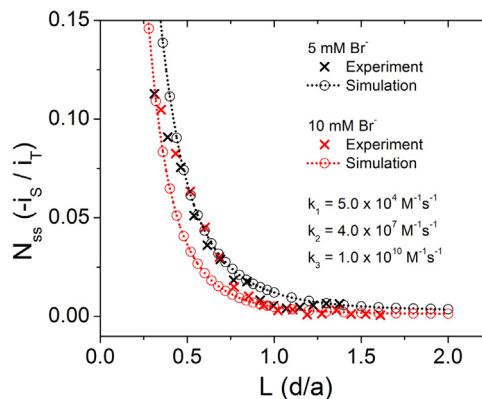


Fig. 5. Experimental and simulated N_{ss} of the intermediate $\text{Br}_2^{\cdot-}$ vs. L (d/a) in 5 and 10 mM Br^- solutions. The simulation results were performed based on the mechanism described in Equations 4–8 using the reactions and corresponding parameters listed in Table 1.

they should. An expanded discussion about these sources of error is provided after Table S1 in the Supporting Information.

Another challenge is determining a unique set of simulation parameters, which hampers our ability to prove which intermediate we are collecting. For example, a simulation using an alternative set of parameters, in which $k_{f,3}$ is much smaller than $1 \times 10^{10} \text{ M}^{-1} \text{ s}^{-1}$ instead of $k_{f,1}$ and $k_{f,2}$, is presented in Fig. S7 and Table S2. This simulation suggests that we are collecting Br_2 because the reaction $\text{Br}_2 + \text{Br}^- \rightleftharpoons \text{Br}_3^-$ is slower than the other homogeneous reactions. On the other hand, the simulation in Fig. 5 and Table 1, where $k_{f,3}$ is $1 \times 10^{10} \text{ M}^{-1} \text{ s}^{-1}$ and $k_{f,1}$ and $k_{f,2}$ are less than $1 \times 10^{10} \text{ M}^{-1} \text{ s}^{-1}$ suggests that we are collecting Br^- . The alternative simulation is potentially valid in that it uses the same reaction pathway and can generate approach curves of the correct magnitude. However, we have more confidence in the parameters in Table 1 because they provide a better fit to the experimental approach curves, which is why we present those parameters as our first choice.

4. Conclusions

In this study, an intermediate formed during the oxidation of Br^- to Br_3^- in NB was detected through SECM, and the mechanism of Br^- oxidation to Br_3^- was proposed to occur through a combined reaction pathway via Br^- , Br_2 and Br_2^- . TG/SC mode in SECM was performed to collect intermediates, and at $d = 3.5 \mu\text{m}$, the N_{ss} polarization curve shows two reduction waves. The wave shown at $E_{\text{sub}} \leq 0.2 \text{ V}$ is attributed to the collection of the stable Br_3^- , and one shown at $0.2 \text{ V} \leq E_{\text{sub}} \leq 0.37 \text{ V}$ is associated with the collection of an unstable intermediate generated in Br^- oxidation. The intermediate was further confirmed by changing d while holding $E_{\text{sub}} = 0.27 \text{ V}$, where only a small amount (<20%) of the generated Br_3^- is collected on the substrate electrode. The N_{ss} started to increase as $L \leq 0.8$ in both 5 and 10 mM Br^- solution, and it reached 0.12, which indicates the collection of an unstable intermediate generated in Br^- oxidation to Br_3^- . The following reaction pathway of Br^- electro-oxidation to Br_3^- was used to simulate the N_{ss} as a function of d in SECM; (1) $\text{Br}^- + e^- \rightleftharpoons \text{Br}^-$, (2) $2\text{Br}^- \rightleftharpoons \text{Br}_2$, (3) $\text{Br}^- + \text{Br}^- \rightleftharpoons \text{Br}_2^-$, (4) $\text{Br}_2 + e^- \rightleftharpoons \text{Br}_2^-$, and (5) $\text{Br}_2 + \text{Br}^- \rightleftharpoons \text{Br}_3^-$. Although the simulation could reproduce the experimental approach curves, it was difficult to discern a unique set of parameters using a mechanism with many adjustable parameters and thereby provide conclusive insight into the identity of the collected intermediates.

Acknowledgements

The authors want to thank Dr. Netzahualcōyotl Arroyo-Currás and Prof. Kevin C. Leonard for help with setting up the cyclic voltammetry experiments and for valuable discussions concerning the reaction mechanisms. The information, data and work presented herein was funded by the Stanford Global Climate and Energy Project (#2777240-51978A). The authors declare no competing financial interest.

Appendix A. Supplementary data

Supplementary data associated with this article can be found, in the online version, at <http://dx.doi.org/10.1016/j.electacta.2017.04.001>.

References

- [1] I.M. Kolthoff, J.F. Coetzee, Polarography in Acetonitrile. II. Metal Ions Which Have Significantly Different Polarographic Properties in Acetonitrile and in Water. Anodic Waves. Voltammetry at Rotated Platinum Electrode, *Journal of the American Chemical Society* 79 (1957) 1852–1858.
- [2] A.I. Popov, D.H. Geske, Studies on the Chemistry of Halogen and of Polyhalides. XVI. Voltammetry of Bromine and Interhalogen Species in Acetonitrile, *Journal of the American Chemical Society* 80 (1958) 5346–5349.
- [3] T. Iwasita, M.C. Giordano, Kinetics of the bromine-tribromide-bromide redox processes on platinum electrodes in acetonitrile solutions, *Electrochimica Acta* 14 (1969) 1045–1059.
- [4] B. Lopez, T. Iwasita, M.C. Giordano, Electrochemical behavior of iodide-iodine and bromide-bromine redox systems in nitromethane solutions, *Journal of Electroanalytical Chemistry and Interfacial Electrochemistry* 47 (1973) 469–478.
- [5] V. Vojinovic, S. Mentus, V. Komnec, Bromide oxidation and bromine reduction in propylene carbonate, *Journal of Electroanalytical Chemistry* 547 (2003) 109–113.
- [6] F. Magno, G.-A. Mazzocchin, G. Bontempelli, Electrochemical behaviour of the bromide ion at a platinum electrode in acetonitrile solvent, *Journal of Electroanalytical Chemistry and Interfacial Electrochemistry* 47 (1973) 461–468.
- [7] W.K. Behl, Anodic Oxidation of Lithium Bromide in Tetrahydrofuran Solutions, *Journal of The Electrochemical Society* 136 (1989) 2305–2310.
- [8] M. Mastragostino, G. Casalbore, S. Valcher, Anodic oxidation of halides in anhydrous acetic acid, *Journal of Electroanalytical Chemistry and Interfacial Electrochemistry* 44 (1973) 37–45.
- [9] J.A. Boon, J.S. Wilkes, J.A. Lanning, An Electrochemical Investigation of the 1-Methyl-3-Ethylimidazolium Bromide Aluminum Bromide Molten Salt System, *Journal of The Electrochemical Society* 138 (1991) 465–469.
- [10] G.D. Allen, M.C. Buzzeo, C. Villagrán, C. Hardacre, R.G. Compton, A mechanistic study of the electro-oxidation of bromide in acetonitrile and the room temperature ionic liquid, 1-butyl-3-methylimidazolium bis(trifluoromethylsulfonyl)imide at platinum electrodes, *Journal of Electroanalytical Chemistry* 575 (2005) 311–320.
- [11] G.D. Allen, M.C. Buzzeo, I.G. Davies, C. Villagrán, C. Hardacre, R.G. Compton, A Comparative Study on the Reactivity of Electrogenerated Bromine with Cyclohexene in Acetonitrile and the Room Temperature Ionic Liquid, 1-Butyl-3-methylimidazolium Bis(trifluoromethylsulfonyl)imide, *The Journal of Physical Chemistry B* 108 (2004) 16322–16327.
- [12] L. Yu, X. Jin, G.Z. Chen, A comparative study of anodic oxidation of bromide and chloride ions on platinum electrodes in 1-butyl-3-methylimidazolium hexafluorophosphate, *Journal of Electroanalytical Chemistry* 688 (2013) 371–378.
- [13] I. Rubinstein, Electrode kinetics of the Br_2/Br^- couple, *The Journal of Physical Chemistry* 85 (1981) 1899–1906.
- [14] A.J. Bard, F.R.F. Fan, J. Kwak, O. Lev, Scanning electrochemical microscopy. Introduction and principles, *Analytical Chemistry* 61 (1989) 132–138.
- [15] M.V. Mirkin, H. Yang, A.J. Bard, Borohydride Oxidation at a Gold Electrode, *Journal of The Electrochemical Society* 139 (1992) 2212–2217.
- [16] F. Zhou, A.J. Bard, Detection of the electrohydrodimerization intermediate acrylonitrile radical anion by scanning electrochemical microscopy, *Journal of the American Chemical Society* 116 (1994) 393–394.
- [17] S. Bi, B. Liu, F.-R.F. Fan, A.J. Bard, Electrochemical Studies of Guanosine in DMF and Detection of Its Radical Cation in a Scanning Electrochemical Microscopy Nanogap Experiment, *Journal of the American Chemical Society* 127 (2005) 3690–3691.
- [18] F. Cao, J. Kim, A.J. Bard, Detection of the Short-Lived Cation Radical Intermediate in the Electrochemical Oxidation of N,N-Dimethylaniline by Scanning Electrochemical Microscopy, *Journal of the American Chemical Society* 136 (2014) 18163–18169.
- [19] J. Chang, A.J. Bard, Detection of the Sn(III) Intermediate and the Mechanism of the Sn(IV)/Sn(II) Electroreduction Reaction in Bromide Media by Cyclic Voltammetry and Scanning Electrochemical Microscopy, *Journal of the American Chemical Society* 136 (2014) 311–320.
- [20] Z. Yang, J. Zhang, M.C.W. Kintner-Meyer, X. Lu, D. Choi, J.P. Lemmon, J. Liu, Electrochemical Energy Storage for Green Grid, *Chem. Rev.* 111 (2011) 3577–3613.
- [21] M. Skyllas-Kazacos, M.H. Chakrabarti, S.A. Hajimolana, F.S. Mjalli, M. Saleem, Progress in Flow Battery Research and Development, *Journal of The Electrochemical Society* 158 (2011) R55–R79.
- [22] C. Ponce de León, A. Frías-Ferrer, J. González-García, D.A. Szánto, F.C. Walsh, Redox flow cells for energy conversion, *Journal of Power Sources* 160 (2006) 716–732.
- [23] M.H. Chakrabarti, R.A.W. Dryfe, E.P.L. Roberts, Evaluation of electrolytes for redox flow battery applications, *Electrochimica Acta* 52 (2007) 2189–2195.
- [24] Q. Liu, A.A. Shinkle, Y. Li, C.W. Monroe, L.T. Thompson, A.E.S. Sleightholme, Non-aqueous chromium acetylacetonate electrolyte for redox flow batteries, *Electrochemistry Communications* 12 (2010) 1634–1637.
- [25] Q. Liu, A.E.S. Sleightholme, A.A. Shinkle, Y. Li, L.T. Thompson, Non-aqueous vanadium acetylacetonate electrolyte for redox flow batteries, *Electrochemistry Communications* 11 (2009) 2312–2315.
- [26] A.E.S. Sleightholme, A.A. Shinkle, Q. Liu, Y. Li, C.W. Monroe, L.T. Thompson, Non-aqueous manganese acetylacetonate electrolyte for redox flow batteries, *Journal of Power Sources* 196 (2011) 5742–5745.
- [27] D.H. Geske, A.H. Maki, Electrochemical Generation of Free Radicals and Their Study by Electron Spin Resonance Spectroscopy; the Nitrobenzene Anion Radical, *Journal of the American Chemical Society* 82 (1960) 2671–2676.
- [28] H. Kojima, A.J. Bard, Determination of rate constants for the electroreduction of aromatic compounds and their correlation with homogeneous electron transfer rates, *Journal of the American Chemical Society* 97 (1975) 6317–6324.

- [29] R.A. Malmsten, H.S. White, Voltammetric Studies beyond the Solvent Limits with Microelectrodes, *Journal of The Electrochemical Society* 133 (1986) 1067–1068.
- [30] R.A. Malmsten, C.P. Smith, H.S. White, Electrochemistry of concentrated organic redox solutions, *Journal of Electroanalytical Chemistry and Interfacial Electrochemistry* 215 (1986) 223–235.
- [31] I. Rubinstein, M. Bixon, E. Gileadi, Confirmation of the hopping mechanism of the conductivity of bromide ions in solutions containing bromine, *The Journal of Physical Chemistry* 84 (1980) 715–721.
- [32] D.W. Peaceman, H.H. Rachford, The Numerical Solution of Parabolic and Elliptic Differential Equations, *Journal of the Society for Industrial and Applied Mathematics* 3 (1955) 28–41.
- [33] A.J. Bard, L.R. Faulkner, *Electrochemical Methods: Fundamentals and Applications*, Wiley, 2000.
- [34] G. Denuault, M.V. Mirkin, A.J. Bard, Direct determination of diffusion coefficients by chronoamperometry at microdisk electrodes, *Journal of Electroanalytical Chemistry and Interfacial Electrochemistry* 308 (1991) 27–38.
- [35] A.J. Bard, M.V. Mirkin, *Scanning Electrochemical Microscopy*, CRC Press, 2001.
- [36] B. Bennett, J. Chang, A.J. Bard, Mechanism of the Br-/Br₂ Redox Reaction on Platinum and Glassy Carbon Electrodes in Nitrobenzene by Cyclic Voltammetry, *Electrochimica Acta* 219 (2016) 1–9.